Aeroelastic Tailoring of a Composite Wing with a Decoupler Pylon as a Wing/Store Flutter Suppressor

I. Lottati*
Technion—Israel Institute of Technology, Haifa, Israel

An analytical investigation was conducted to determine the influence of the decoupler pylon on the aeroelastic behavior of a composite, rectangular wing. It is assumed that the wing is carrying a fuselage at its semispan and an external store attached to a decoupler pylon at a various station along the wing's span and that the aircraft is in a free-flight condition (unrestrained vehicle). Passive soft-spring/damper elements are used to decouple wing modes from store pitch modes. The effect of some parameters on the ability of the decoupler pylon to suppress flutter are analyzed. It is shown by analysis that the decoupler pylon provides substantial increase in flutter speed and that the ability of the decoupler pylon to suppress flutter is influenced mainly by the spanwise and chordwise pivot point location of the external attached store. Furthermore, it is shown that the aeroelastic tailoring of the wing and angle of sweep have a major influence on the flutter instability of the configuration.

Introduction

HIGH-PERFORMANCE aircraft are required to carry many combinations of external wing-mounted stores. Some of these stores are critical from the design standpoint of preventing dangerous aeroelastic instabilities within the required operational flight envelope. Flutter can be prevented passively by either relocating the store spanwise and/or chordwise or by tuning the pylon stiffness characteristics.[1-4] The flutter speed can be raised by applying more advanced methods involving active control technology.[5-8] The decoupler pylon[4] is a new passive system that has been shown in exploratory studies to be effective in suppressing wing/store flutter instability. The decoupler pylon dynamically isolates (or behaves like a vibration absorber or as a decoupler) the wing from store pitch inertia effects by providing a low store pitch frequency. Flight tests[9] conducted by the decoupler pylon recently demonstrated the ability of this passive method to suppress wing/store flutter instability.

In this paper, the effectiveness of the decoupler pylon is demonstrated by analysis for a free-free aircraft and the results of parametric study by variation of some important parameters that affect flutter are presented.

Aeroelastic Analysis of the Free Aircraft with Decoupler Pylon

This analysis considers a high-aspect-ratio rectangular swept wing. The uniform rectangular wing is taken as a beam-like surface carrying a fuselage at the semispan and concentrated store attached to a decoupler pylon at various stations along the wing's span (see Fig. 1). It is assumed that the resulting box-beam wing structure is such that its deformation may be presented by a bending deflection $h(y)$, positive downward, along a straight reference axis (axis of rotation) and a rotation $\alpha(y)$, positive nose up, about this axis (see Fig. 2c). In addition, it is further assumed that the wing chordwise sections, perpendicular to the beam's reference axis, are rigid so that the wing deformation is a function only of the spanwise coordinates y. A schematic illustration of the decoupler pylon system studied herein is shown in Fig. 1. The store is pivoted by an angle β around a pivot point, which is not necessarily the same as α in this spanwise location. Frequency and damping of the store pitch mode are controlled by passive spring/dashpot elements.

As stated, the deformation of the wing is assumed of the form

$$w(x,y) = h(y) + X_a \alpha(y) \tag{1}$$

where $X_a = x - b \cdot a$.

Using the box-beam model, the equivalent bending and torsion stiffnesses EI_b and GJ, respectively, may be computed by employing the strain energy method. The strain energy U for a symmetric anisotropic laminated plate is given as[10]

$$U = \frac{1}{2}\int_0^l \int_{-b}^{b} \left[D_{11}\left(\frac{\partial^2 w}{\partial x^2}\right)^2 + 2D_{12}\frac{\partial^2 w}{\partial x^2}\frac{\partial^2 w}{\partial y^2} + D_{22}\left(\frac{\partial^2 w}{\partial y^2}\right)^2 + 4D_{16}\frac{\partial^2 w}{\partial x^2}\frac{\partial^2 w}{\partial x \partial y} + 4D_{26}\frac{\partial^2 w}{\partial y^2}\frac{\partial^2 w}{\partial x \partial y} + 4D_{66}\left(\frac{\partial^2 w}{\partial x \partial y}\right)^2 \right] dx\,dy + \frac{1}{2}K_{fp}X_p^2(\alpha_{l_p} - \beta)^2 \tag{2}$$

where D_{ij} are the flexural moduli for N ply laminate with ply angle orientation θ and w the transverse deflection of the plate, positive downward (see Fig. 2b). α_{l_p} stands for angle of attack of the wing at the $y = l_p$ spanwise location.

The kinetic energy of the system is given by

$$T = \frac{1}{2}\int_0^l \int_{-b}^{b} \rho(x,y)\left(\frac{\partial w}{\partial t}\right)^2 dx\,dy + \frac{1}{2}\int_{bf_1}^{bf_2} \rho_f(x)\left(\frac{\partial w}{\partial t}\bigg|_{y=0}\right)^2 dx + \frac{1}{2}\int_{bp_1}^{bp_2} \rho_p(x)\left(\frac{\partial w}{\partial t}\bigg|_{y=l_p}\right)^2 dx \tag{3}$$

where $\rho(x,y)$ is the material density of the wing and $\rho_p(x)$ and $\rho_f(x)$ the density of the pylon and fuselage, respectively. b_{p_1} and b_{p_2} are the forward and the rearward coordinates of

Received July 11, 1986; revision received April 15, 1987.

*Senior Lecturer, Department of Aeronautical Engineering.

the pylon, while b_{f_1} and b_{f_2} represent the fuselage coordinates, respectively.

The deflection of the store is given by

$$w|_{y=l_p} = h_{l_p} + X_{fp}(\beta - \alpha_{l_p}) + X_a\beta \tag{4}$$

where h_{l_p} is the wing bending deflection at the wing's axis of rotation at the $y=l_p$ spanwise location.

The virtual work expression is given by

$$\delta w = \int_0^l (-L\delta h + M\delta\alpha)\mathrm{d}y \tag{5}$$

where L is the aerodynamic lift, positive upward, and M the aerodynamic moment about the wing axis of rotation, positive nose up. The aerodynamic forces due to the fuselage and pylon are not taken into account in the analysis. The aerodynamic forces due to the store are very difficult to assess and usually they are omitted (see Refs. 4, 12, and 13).

Applying the principle of minimum potential energy, one gets the following governing differential equations of motion:

$$EI_b\frac{\partial^4 h}{\partial y^4} + d_{22}\frac{\partial^4\alpha}{\partial y^4} + K\frac{\partial^3\alpha}{\partial y^3} + m\frac{\partial^2 h}{\partial t^2} + mX_\alpha\frac{\partial^2\alpha}{\partial t^2} = -L$$

$$d_{22}\frac{\partial^4 h}{\partial y^4} - K\frac{\partial^3 h}{\partial y^3} + S\frac{\partial^4\alpha}{\partial y^4} - GJ\frac{\partial^2\alpha}{\partial y^2} + mX_\alpha\frac{\partial^2 h}{\partial t^2} + I_\alpha\frac{\partial^2\alpha}{\partial t^2} = M \tag{6}$$

where

m = mass per unit span, $= \int_{-b}^{b}\rho\mathrm{d}x$

EI_b = beam bending stiffness, $= \int_{-b}^{b} D_{22}\mathrm{d}x$

GJ = torsional stiffness, $= 4\int_{-b}^{b} D_{66}\mathrm{d}x$

K = bending-torsion cross-coupling stiffness, $= 2\int_{-b}^{b} D_{26}\mathrm{d}x$
A positive K provides a wash-in elastic coupling (bending up/twist up or $-\Delta h/+\Delta\alpha$)

S = torsional stiffness due to rigidity in tension (warping effect), $= \int_{-b}^{b} D_{22}X_a{}^2\mathrm{d}x$

X_α = section mass moment of inertia (per unit span) about wing axis of rotation, $= \left(\int_{-b}^{b}\rho X_a\mathrm{d}x\right)\Big/m$

I_α = section mass moment of inertia of wing (per unit span) about wing axis of rotation, $= \int_{-b}^{b}\rho X_a^2\mathrm{d}x$

d_{22} = coupling term due to $a\neq 0$, $= \int_{-b}^{b} D_{22}X_a\mathrm{d}x = -abEI_b$

d_{26} = coupling term due to $a\neq 0$, $= 2\int_{-b}^{b} D_{26}X_a\mathrm{d}x = -abK$

To get the boundary conditions for this system and to take into account the concentrated mass at $y=l_p$, it is essential to

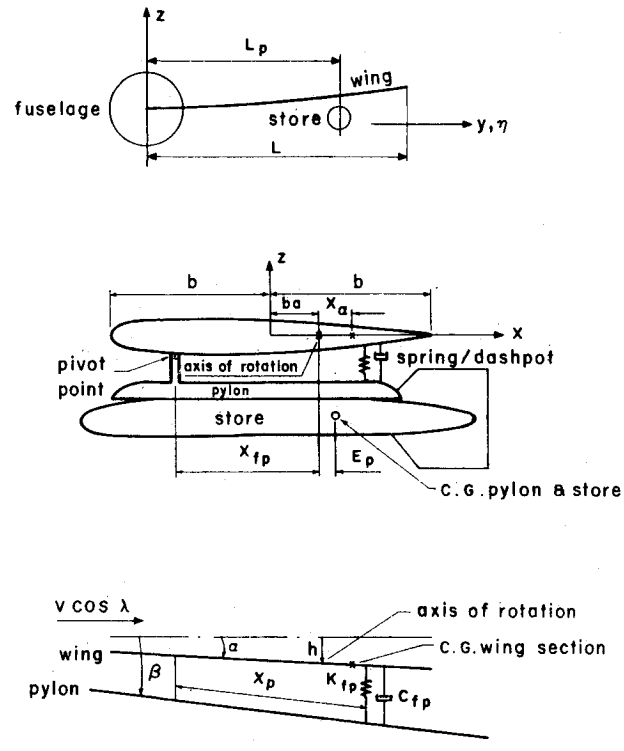

Fig. 1 Wing and decoupler pylon system and geometrical definition.

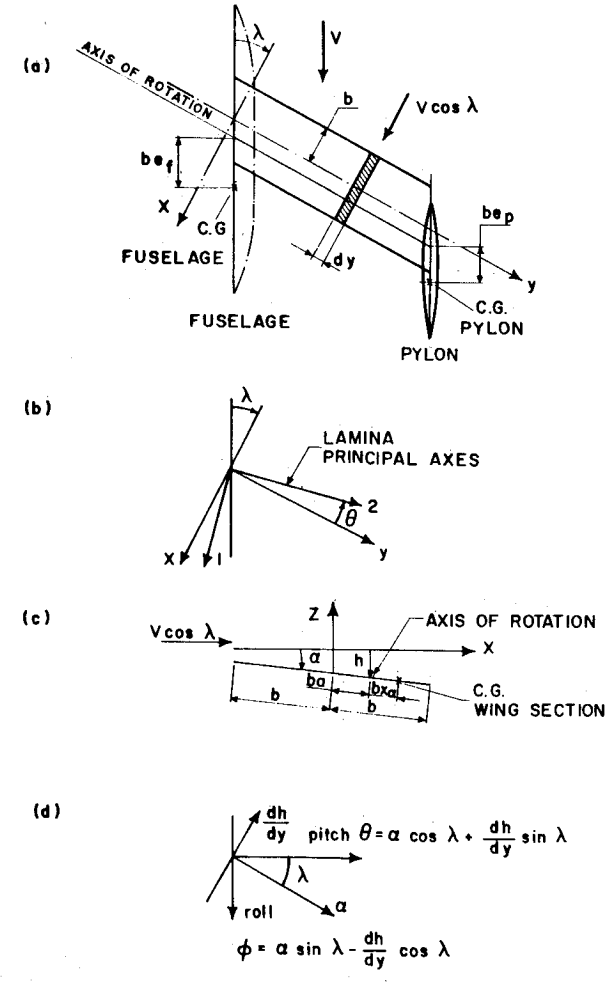

Fig. 2 Slender swept wing planform, lamina orientation, displacement assumptions, and a vector diagram of the elastic deformation and the pitch and roll of a swept wing.

split each of the integrals of the potential and kinetic energy [Eqs. (2) and (3)] into two subintegrals, namely,

$$\int_0^l l\mathrm{d}y = \int_0^{l_p} l\mathrm{d}y + \int_{l_p}^{l} l\mathrm{d}y \tag{7}$$

Performing the necessary algebraic steps, one gets the boundary conditions for the unrestrained aircraft. For $y=0$ (root section),

shear condition

$$EI_b\frac{\partial^3 h}{\partial y^3} + d_{22}\frac{\partial^3 \alpha}{\partial y^3} + K\frac{\partial^2 \alpha}{\partial y^2} + M_f\left(\frac{\partial^2 h}{\partial t^2} + E_f\frac{\partial^2 \alpha/\partial t^2}{\cos\lambda}\right) = 0 \tag{8a}$$

torque and moment condition

$$\cos\lambda\left(d_{22}\frac{\partial^3 h}{\partial y^3} - K\frac{\partial^2 h}{\partial y^2} + S\frac{\partial^3 \alpha}{\partial y^3} - GJ\frac{\partial \alpha}{\partial y}\right) - \sin\lambda\left(EI_b\frac{\partial^2 h}{\partial y^2} + d_{22}\frac{\partial^2 \alpha}{\partial y^2} + K\frac{\partial \alpha}{\partial y}\right) + M_f\left(E_f\frac{\partial^2 h}{\partial t^2} + K_f{}^2\frac{\partial^2 \alpha/\partial t^2}{\cos\lambda}\right) = 0 \tag{8b}$$

no roll condition

$$-\cos\lambda\frac{\partial h}{\partial y} + \sin\lambda\ \alpha = 0 \tag{8c}$$

warping condition

$$d_{22}\frac{\partial^2 h}{\partial y^2} + S\frac{\partial^2 \alpha}{\partial y^2} + d_{26}\frac{\partial \alpha}{\partial y} = 0 \tag{8d}$$

where M_f is half of the mass of the fuselage, E_f the distance that the center of gravity of fuselage lies behind the wing axis of rotation, and K_f the radius of gyration of the fuselage about the wing axis of rotation. Furthermore λ is the wing's angle of sweep, positive backward.

The boundary conditions at the wing tip ($y=l$) are

shear condition

$$EI_b\frac{\partial^3 h}{\partial y^3} + d_{22}\frac{\partial^3 \alpha}{\partial y^3} + K\frac{\partial^2 \alpha}{\partial y^2} = 0 \tag{9a}$$

torque condition

$$-d_{22}\frac{\partial^3 h}{\partial y^3} + K\frac{\partial^2 h}{\partial y^2} - S\frac{\partial^3 \alpha}{\partial y^3} + GJ\frac{\partial \alpha}{\partial y} = 0 \tag{9b}$$

moment condition

$$EI_b\frac{\partial^2 h}{\partial y^2} + d_{22}\frac{\partial^2 \alpha}{\partial y^2} + K\frac{\partial \alpha}{\partial y} = 0 \tag{9c}$$

warping condition

$$d_{22}\frac{\partial^2 h}{\partial y^2} + S\frac{\partial^2 \alpha}{\partial y^2} + d_{26}\frac{\partial \alpha}{\partial y} = 0 \tag{9d}$$

The concentrated mass at $y=l_p$ causes a discontinuity of the shear, torque, and moment that are of the form (ϵ stands for an infinitesimal small distance),

shear condition

$$\left(EI_b\frac{\partial^3 h}{\partial y^3} + d_{22}\frac{\partial^3 \alpha}{\partial y^3} + K\frac{\partial^2 \alpha}{\partial y^2}\right)_{l_p-\epsilon} - \left(EI_b\frac{\partial^3 h}{\partial y^3} + d_{22}\frac{\partial^3 \alpha}{\partial y^3} + K\frac{\partial^2 \alpha}{\partial y^2}\right)_{l_p+\epsilon} - M_p\left[\frac{\partial^2 h}{\partial t^2} - X_{fp}\left(\cos\lambda\frac{\partial^2 \alpha}{\partial t^2} + \sin\lambda\frac{\partial^3 h}{\partial y\partial t^2}\right) + (X_{fp}+E_P)\frac{\partial^2 \beta}{\partial t^2}\right]_{y=l_p} = 0 \tag{10a}$$

torque and moment condition

$$\left(-d_{22}\frac{\partial^3 h}{\partial y^3} + K\frac{\partial^2 h}{\partial y^2} - S\frac{\partial^3 \alpha}{\partial y^3} + GJ\frac{\partial \alpha}{\partial y}\right)_{l_p-\epsilon} - \left(-d_{22}\frac{\partial^3 h}{\partial y^3} + K\frac{\partial^2 h}{\partial y^2} - S\frac{\partial^3 \alpha}{\partial y^3} + GJ\frac{\partial \alpha}{\partial y}\right)_{l_p+\epsilon} + M_p\cos\lambda\left[E_P\frac{\partial^2 h}{\partial t^2} - X_{fp}E_p\left(\cos\lambda\frac{\partial^2 \alpha}{\partial t^2} + \sin\lambda\frac{\partial^3 h}{\partial y\partial t^2}\right) + (X_{fp}E_p + K_p^2)\frac{\partial^2 \beta}{\partial t^2}\right]_{y=l_p} = 0 \tag{10b}$$

moment condition

$$\left(EI_b\frac{\partial^2 h}{\partial y^2} + d_{22}\frac{\partial^2 \alpha}{\partial y^2} + K\frac{\partial \alpha}{\partial y}\right)_{l_p-\epsilon} - \left(EI_b\frac{\partial^2 h}{\partial y^2} + d_{22}\frac{\partial^2 \alpha}{\partial y^2} + K\frac{\partial \alpha}{\partial y}\right)_{l_p+\epsilon} + M_p\sin\lambda\left[E_p\frac{\partial^2 h}{\partial t^2} - X_{fp}E_p\left(\cos\lambda\frac{\partial^2 \alpha}{\partial t^2} + \sin\lambda\frac{\partial^3 h}{\partial y\partial t^2}\right) + (X_{fp}E_p + K_p^2)\frac{\partial^2 \beta}{\partial t^2}\right]_{y=l_p} = 0 \tag{10c}$$

warping condition

$$\left(d_{22}\frac{\partial^2 h}{\partial y^2} + S\frac{\partial^2 \alpha}{\partial y^2} + d_{26}\frac{\partial \alpha}{\partial y}\right)_{l_p-\epsilon} - \left(d_{22}\frac{\partial^2 h}{\partial y^2} + S\frac{\partial^2 \alpha}{\partial y^2} + d_{26}\frac{\partial \alpha}{\partial y}\right)_{l_p+\epsilon} = 0 \tag{10d}$$

where M_p is the mass of the pylon and store, E_p the distance that the center of gravity of the pylon and store lies behind the wing axis of rotation, and K_p the radius of gyration of the pylon and store about the wing axis of rotation.

On the other hand, h, $\partial h/\partial y$, α, and $\partial\alpha/\partial y$ are continuous across $y=l_p$. Hence,

$$[h]_{l_p-\epsilon} = [h]_{l_p+\epsilon};\quad \left[\frac{\partial h}{\partial y}\right]_{l_p-\epsilon} = \left[\frac{\partial h}{\partial y}\right]_{l_p+\epsilon}$$

$$[\alpha]_{l_p-\epsilon} = [\alpha]_{l_p+\epsilon};\quad \left[\frac{\partial \alpha}{\partial y}\right]_{l_p-\epsilon} = \left[\frac{\partial \alpha}{\partial y}\right]_{l_p+\epsilon} \tag{11}$$

The α and h (of the wing) at $y=l_p$ are related to β (pitch angle of the store) in the form

$$K_{fp}X_p^2\beta + M_p(X_{fp}^2 + 2X_{fp}E_p + K_p^2)\frac{\partial^2\beta}{\partial t^2}$$

$$= K_{fp}X_p^2\left(\cos\lambda\alpha + \sin\lambda\frac{\partial h}{\partial y}\right) - M_p(X_{fp}+E_p)$$

$$\times\left[\frac{\partial^2 h}{\partial t^2} - X_{fp}\left(\cos\lambda\frac{\partial^2\alpha}{\partial t^2} + \sin\lambda\frac{\partial^3 h}{\partial y\,\partial t^2}\right)\right] \quad (12)$$

The aerodynamics required to solve these aeroelastic equations generally varies in levels of sophistication. Due to the complexity of the problem and in order to establish trends, the unsteady aerodynamic strip theory[14] shall be employed. The expressions for the aerodynamic forces are given in Ref. 15, as well as the expression for the approximation of the Theodorsen function $C(k)$ applied in the analysis.

The problem is solved exactly assuming an exact solution of the forms

$$\frac{h}{b} = \sum_{i=1}^{8} H_i e^{r_i\eta}e^{\sigma\tau} \text{ and } \alpha = \sum_{i=1}^{8} A_i e^{r_i\eta}e^{\sigma\tau} \text{ for } \eta<\eta_p \quad (13a)$$

and

$$\frac{h}{b} = \sum_{i=9}^{16} H_i e^{r_i\eta}e^{\sigma\tau} \text{ and } \alpha = \sum_{i=9}^{16} A_i e^{r_i\eta}e^{\sigma\tau} \text{ for } \eta>\eta_p \quad (13b)$$

where $\eta=y/l$ and $\tau=\sqrt{EI_b/ml^4}\,t$ are the nondimensional spanwise coordinate and time, respectively, and $\sigma=\delta+i\omega$, where δ is the damping and ω the frequency of the oscillating wing (δ and ω assumed real). Furthermore, $\eta_p=l_p/l$ the nondimensional spanwise location of the pylon and store.

The 16 H_i and A_i unknown constants should be adjusted so as to satisfy the boundary conditions given by Eqs. (8-11).

Incorporating the expressions for the assumed solution [Eqs. (13)] in the governing equations (6) and the boundary conditions [Eqs. (8-11)], one gets the following nondimensional set of equations:

$$(r^4+\sigma^2+QL_h)H + (-ar^4+k_\alpha r^3+x_\alpha\sigma^2+QL_\alpha)A = 0 \quad (14a)$$

$$(-ar^4-k_\alpha r^3+x_\alpha\sigma^2-QM_h)H + (s_\alpha r^4-g_\theta r^2+I_\theta\sigma^2-QM_\alpha)A = 0 \quad (14b)$$

$$-r\cos\lambda H + AR\sin\lambda A = 0 \quad (15c)$$

$$-ar^2H + (s_\alpha r^2 - ak_\alpha r)A = 0 \quad (15d)$$

where $m_f=M_f/ml$, $e_f=E_f/b$, and $k_f=K_f/b$.

For $\eta=1$ (wing tip), the boundary conditions are

$$[r^3H + (-ar^3+k_\alpha r^2)A]e^r = 0 \quad (16a)$$

$$[(-ar^3-k_\alpha r^2)H + (s_\alpha r^3-g_\theta r)A]e^r = 0 \quad (16b)$$

$$[r^2H + (-ar^2+k_\alpha r)A]e^r = 0 \quad (16c)$$

$$[-ar^2H + (s_\alpha r^2-ak_\alpha r)A]e^r = 0 \quad (16d)$$

and for $\eta=\eta_p$ (pylon spanwise location)

$$\{[r^3H + (-ar^3+k_\alpha r^2)A]_{\eta_p-\epsilon} - [r^3H + (-ar^3+k_\alpha r^2)A]_{\eta_p+\epsilon} - m_p\sigma^2[(1+e_p r\sin\lambda/AR)H + e_p\cos\lambda A]\}e^{r\eta_p} = 0 \quad (17a)$$

$$\{[(-ar^3-k_\alpha r^2)H + (s_\alpha r^3-g_\theta r)A]_{\eta_p-\epsilon} - [(-ar^3-k_\alpha r^2)H + (s_\alpha r^3-g_\theta r)A]_{\eta_p+\epsilon} - m_p\cos\lambda\sigma^2[(e_p+k_p{}^2 r\sin\lambda/AR)H + k_p{}^2\cos\lambda A]\}e^{r\eta_p} = 0 \quad (17b)$$

$$\{[r^2H + (-ar^2+k_\alpha r)A]_{\eta_p-\epsilon} - [r^2H + (-ar^2+k_\alpha r)A]_{\eta_p+\epsilon} + m_p(\sin\lambda/AR)\sigma^2[(e_p+k_p{}^2 r\sin\lambda/AR)H + k_p{}^2\cos\lambda A]\}e^{r\eta_p} = 0 \quad (17c)$$

$$\{[-ar^2H + (s_\alpha r^2-ak_\alpha r)A]_{\eta_p-\epsilon} - [-ar^2H + (s_\alpha r^2-ak_\alpha r)A]_{\eta_p+\epsilon}\}e^{r\eta_p} = 0 \quad (17d)$$

where $m_p=M_p/ml$, $e_p=E_p/b$, $k_p=K_p/b$, and

$$([H]_{\eta_p-\epsilon} - [H]_{\eta_p+\epsilon})e^{r\eta_t} = 0$$

$$([rH]_{\eta_p-\epsilon} - [rH]_{\eta_p+\epsilon})e^{r\eta_p} = 0$$

$$([A]_{\eta_p-\epsilon} - [A]_{\eta_p+\epsilon})e^{r\eta_p} = 0$$

$$([rA]_{\eta_p-\epsilon} - [rA]_{\eta_p+\epsilon})e^{r\eta_p} = 0 \quad (18)$$

The pitch angle of the pylon β is related to the motion of wing in the form (assuming $\beta=Be^{r\eta_p}e^{\sigma\tau}$)

$$B = \frac{\omega_p(\omega_p+2\xi_p\sigma)[\cos\lambda A + (\sin\lambda/AR)rH] - (x_{fp}+e_p)\sigma^2\{H - x_{fp}[\cos\lambda A + (\sin\lambda/AR)rH]\}}{\omega_p(\omega_p+2\xi_p\sigma) + \sigma^2(x_{fp}^2 + 2x_{fp}e_p + k_p^2)} \quad (19)$$

where

$$x_\alpha = X_\alpha/b,\ AR = l/b,\ k_\theta = K/EI_b$$

$$k_\alpha = k_\theta AR,\ s_\alpha = S/b^2EI_b,\ g_g = GJ/EI_b$$

$$g_\theta = g_g(AR)^2,\ I_\theta = I_\alpha/mb^2,\ Q = \pi\rho v^2 l^4/EI_b$$

$$x_{fp} = X_{fp}/b,\ x_p = X_p/b$$

where L_h, L_α, M_h, and M_α are the aerodynamic coefficients (given in Ref. 15).

The boundary conditions, given in a nondimensional form, for $\eta=0$ (root section) are

$$r^3H + (-ar^3+k_\alpha r^2)A + m_f\sigma^2(H+e_fA/\cos\lambda) = 0 \quad (15a)$$

$$\cos\lambda[(-ar^3-k_\alpha r^2)H + (s_\alpha r^3-g_\theta r)A] + AR\sin\lambda[-r^2H + (ar^2-k_\alpha r)A] + m_f\sigma^2(e_fH + k_f{}^2A/\cos\lambda) = 0 \quad (15b)$$

where $\omega_p^2=K_{fp}X_p^2/M_p$ is the store and pylon natural frequency and $2\xi_p\omega_p=C_{fp}X_p^2/M_p$ the dashpot damping coefficient.

It should be noted that the damping of the store pitch mode ξ_p is incorporated in the analysis by analyzing forces and moments acting on the store and wing.

To obtain a nontrivial solution, the determinant of the system of Eqs. (14) has to be zero [$\Delta(r,\sigma)=0$, forming the characteristic polynomials in r and σ of the problem]. For prescribed σ, the zero determinant condition [$\Delta(r,\sigma)=0$] has to be applied to obtain the root r_i of the characteristic polynomials of the system. The roots r_i with the prescribed σ has to satisfy the boundary conditions given by Eqs. (15-18). Thus, to satisfy the boundary conditions, the determinant of the set of linear equations (15-18) has to be equal to zero [$\Delta_b(r,\sigma)=0$] to reach a nontrivial solution.

The combination of ω and Q (minimum) fulfilling the conditions $\Delta(r,\sigma)=0$ and $\Delta_b(r,\sigma)=0$ so as to bring the system

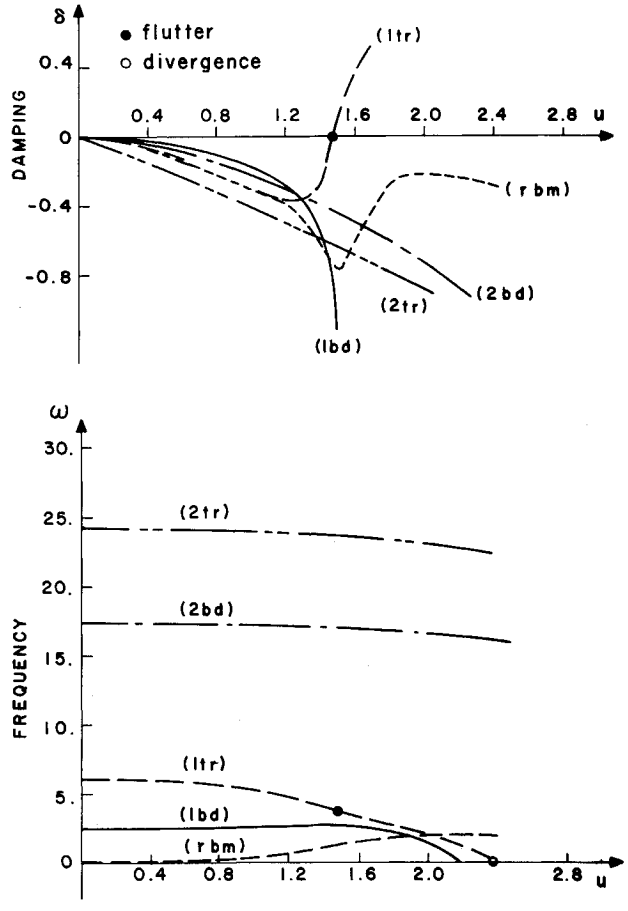

Fig. 3 Frequency and damping of the fundamental aeroelastic modes (first and second bending and torsion) and the rigid-body mode vs dimensionless airspeed for a rigid pylon mounted at the tip of an unswept wing.

Table 1 Properties of rectangular wing ($AR=6.16$)

$m=149.5$ lb	$l=19.4$ ft
$EI_b=18.09\times10^6$ lb·ft^2	$x_\alpha=0.16$
$GJ=4.68\times10^6$ lb·ft^2	$a=-0.36$
$\rho=2.3769\times10^{-3}$ slug/ft^3	$e_f=-0.455$
$m_f=1.2757$	$e_p=0$
$m_p=0.3641$	$k_f=2.2759$
$b=3.15$ ft	$k_p=0.6603$

from neutral stability ($\delta=0$) to instability ($\delta>0$) are the conditions at which the wing will undergo dynamic ($\omega\neq0$) or static ($\omega=0$) instability. The numerical procedure of the solution is outlined in the Appendix of Ref. 15

It should be stated that the rigid-body modes are affecting the dynamic system through the boundary conditions at the root section of the wing. The ability of the fuselage to oscillate in pitch and heave simulates what is usually referred to as the rigid-body modes of the unrestrained vehicle.

Applications

The difficulties involved in investigating the flutter of a system is the large number of possible parameters affecting the analysis. The numerical example given by Goland and Luke[16] is selected as a case study. This example consists of an aircraft having a rigid fuselage and carrying a store attached to a pylon in various spanwise wing locations in a symmetric free flight (unrestrained vehicle). The vehicle has a uniform rectangular wing (AR = 6.16) of constant mass per unit span with the properties listed in Table 1.

This numerical example was studied among others by Housner and Stein[17] and Lottati.[11] The study herein is conducted while taking into account the d_{22},d_{26}, and warping term s_α.

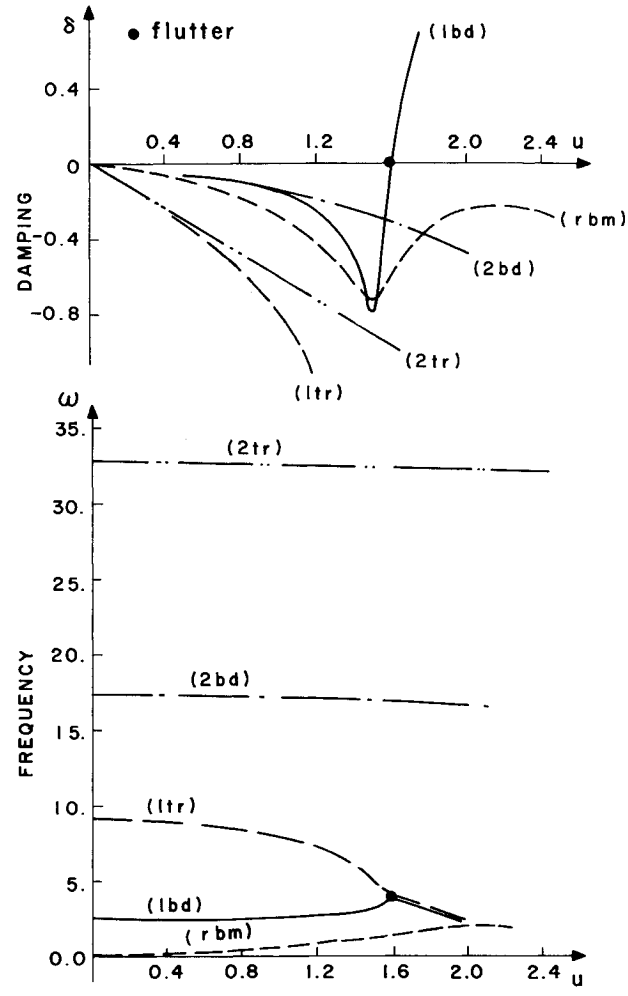

Fig. 4 Frequency and damping of the fundamental aeroelastic modes and the rigid-body mode vs dimensionless airspeed for a soft decoupler pylon mounted at the tip of an unswept wing ($\omega_p=0.5$, $x_{fp}=0$, $\xi_p=0$).

The configuration of the rigid pylon (and store) at the tip is taken as reference. Figure 3 presents the variation of the frequencies and damping of the first and second bending and torsion elastic modes and the rigid-body mode vs the nondimensional velocity of the flow ($u=v/v_{\text{ref}}$, where $v_{\text{ref}}=400$ mph) for the pylon mounted rigidly. Figure 3 illustrates how the frequency of the first torsion mode (1tr) drops while increasing the velocity u until it interacts with the first bending mode (1bd) and fluttered at $u_{cr}=1.47$ $\omega_{cr}=3.637$.

To test the ability of the decoupler pylon to suppress flutter instability, the spring is softened to get a "soft" decoupler pylon of $\omega_p=0.5$ without damping ($\xi_p=0$) and $x_{fp}=0$ (pivot point located at the wing axis of rotation). Figure 4 shows the variation of frequencies and damping of the elastic and rigid-body modes of the system. Figure 4 illustrates a classical interaction of the 1bd and 1tr modes to develop flutter instability at $u_{cr}=1.598$, $\omega_{cr}=3.841$.

Figure 5 presents the variation of the frequencies and damping of the modes vs the velocity of the flow for a "tuned" decoupler with $\omega_p=4$ and without damping ($\xi_p=0$) and $x_{fp}=0$. The results of Fig. 5 show that the frequency of the 1tr mode is decoupled from the 1bd mode as expected (see Ref. 4) and fluttered at a very high velocity (beyond the range of scale in Fig. 5), but the pylon mode (pym) interacts with the 1bd mode to undergo flutter at $u_{cr}=1.411$, $\omega_{cr}=3.545$. It should be noted that the amplitude of the pitch angle of the pylon β may approach infinity, indicating resonance when

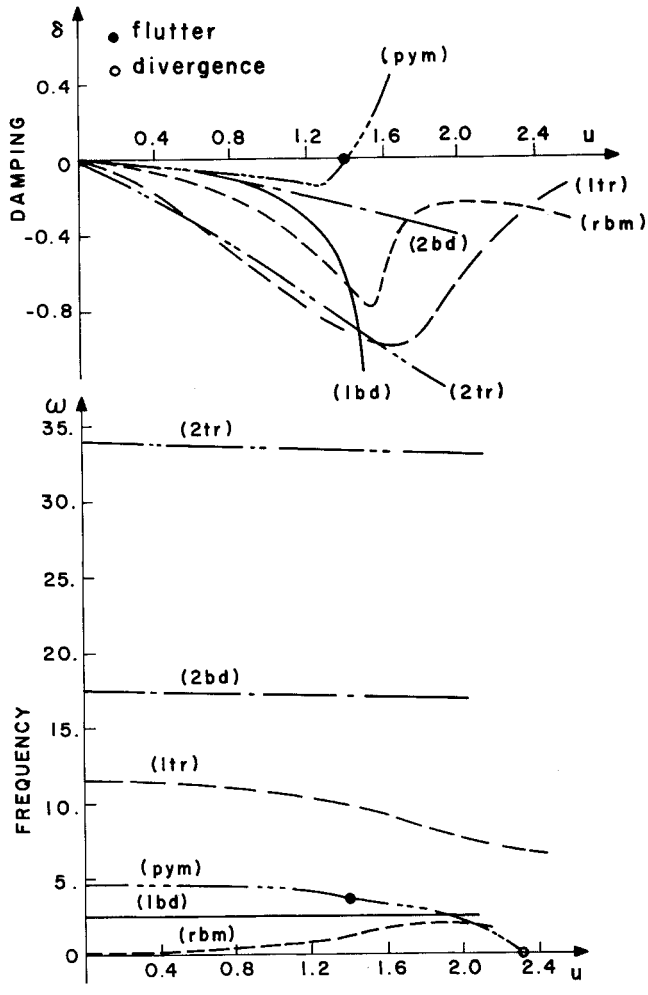

Fig. 5 Frequency and damping of the fundamental aeroelastic modes, rigid mode and pylon mode vs dimensionless airspeed for a tuned decoupler pylon mounted at the tip of an unswept wing ($\omega_p = 4$, $x_{fp} = 0$, $\xi_p = 0$).

[see Eq. (19), assuming no damping $\xi_p = 0$],

$$\sigma^2 = -\omega_p^2/(x_{fp}^2 + 2x_{fp}e_p + k_p^2) \tag{20}$$

The ltr mode does not flutter due to the fact that the pylon is behaving as a vibration absorber. The pym mode is not plotted in Fig. 3 due to the fact that, for a rigid pylon, the frequency of pym is infinity large. Furthermore, the pylon mode is not plotted in Fig. 4 due to the fact that, for a soft decoupler pylon, the frequency and damping of the pym mode is too low to be traced.

Figure 6 depicts the critical frequency and velocity at flutter vs the spring natural frequency ω_p of the decoupler pylon. The results of Fig. 6 show that the system with the tuned pylon [$0.7 < (\omega_p/\omega_{h1}) < 1.5$, where $\omega_{h1} = 3.52$ is approximately the frequency of the 1bd mode of the system at vacuo] will undergo flutter instability at about the same flutter velocity as the system with the rigid pylon. The very same conclusion may be drawn from Fig. 7, which shows the critical frequency and velocity at flutter vs the spring natural frequency ω_p for a pylon at $\eta_p = 0.5$ of the wing's spanwise allocation. The flutter velocity of the system with the pylon allocate at $\eta_p = 0.5$ is lower than the critical velocity for the system with the pylon allocate allocate at the tip ($\eta_p = 1$). The results of Figs. 4-7 indicate that, for zero x_{fp} (pivot pylon allocate at the rotation axis), the decoupler pylon is not effective as a passive flutter suppressor.

Figure 8 illustrates the variation of the flutter velocity of the system vs the natural frequency of the spring ω_p for

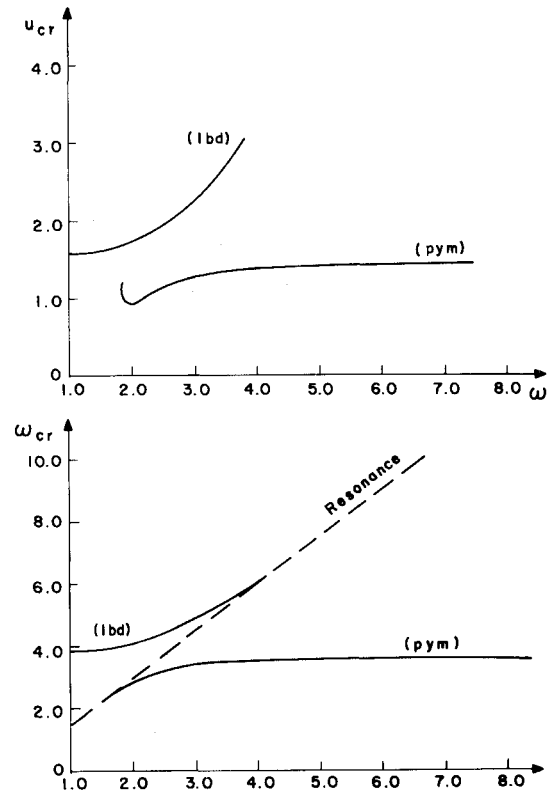

Fig. 6 Variation of the critical frequency and velocity of the system vs the natural frequency of the decoupler pylon's spring while the store is mounted at the tip of an unswept wing ($\xi_p = 0$, $x_{fp} = 0$).

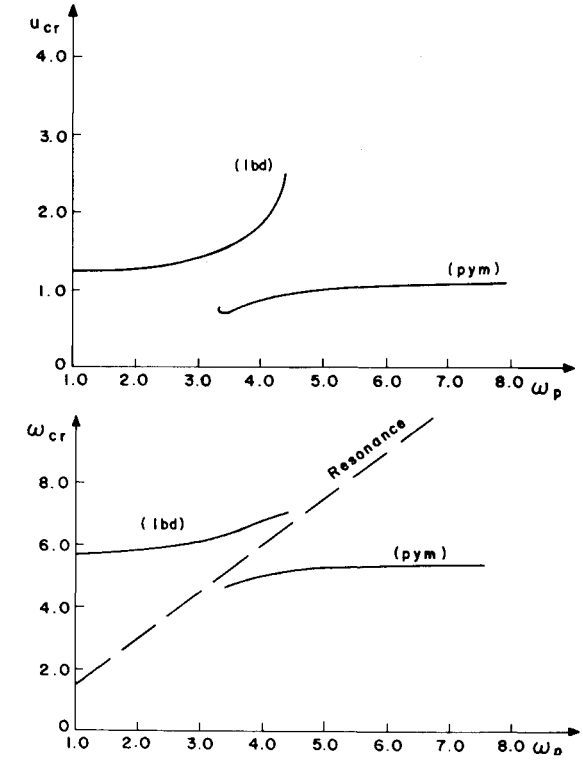

Fig. 7 Variation of the critical frequency and velocity of the system vs the natural frequency of the decoupler pylon's spring while the store is mounted at the middle of the semispan of an unswept wing ($\xi_p = 0$, $x_{fp} = 0$).

various values of damping coefficient ($x_{fp} = 0$ and the pylon allocate at the tip $\eta_p = 1$). The results of Fig. 8 show that, for a zero damping coefficient ($\xi_p = 0$), the curve of the flutter

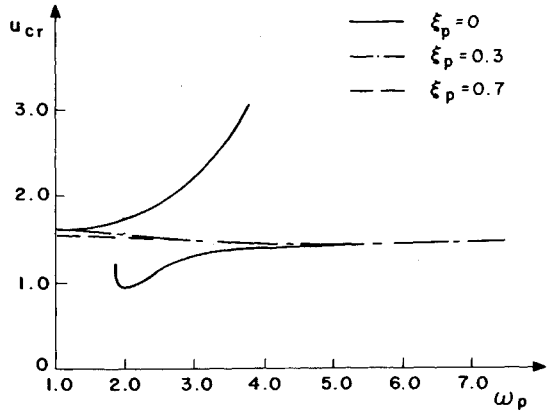

Fig. 8 Variation of the critical velocity of the system vs the natural frequency of the decoupler pylon's spring while the store is mounted at the wing's tip for various values of the dashpot damping coefficient ($x_{fp} = 0$) for an unswept wing.

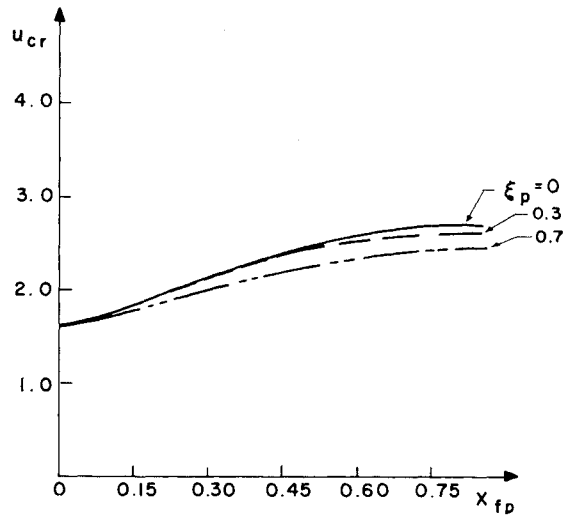

Fig. 9 Variation of the critical velocity of the system vs the location of the decoupler pylon's pivot point while the store is mounted at the wing's tip for various values of the dashpot damping coefficient ($\omega_p = 0.5$) for an unswept wing.

velocity is a discontinuous one with respect to ω_p due to the resonance phenomena shown in Figs. 6 and 7. For $\xi_p > 0$, the variation of the flutter velocity is a continuous curve with respect to ω_p. The results of Fig. 8 indicate that the damping does not affect the flutter velocity of the systems.

The variation of the flutter velocity of the system vs the variation of the pivot point x_{fp} for various values of the damping coefficient is shown in Fig. 9 ($\omega_p = 0.5, \eta_p = 1$). The results of Fig. 9 reveal that the location of the pivot point (x_{fp} parameter) has a significant influence on the flutter velocity of the system. Moving the pivot point forward considerably increases the flutter velocity of the system. Flight tests made to test the ability of the decoupler pylon to suppress flutter are reported in Ref. 9. The flight tests were conducted with pylons that use a unique two-link pivoting arrangement which functions as a virtual or remote pitch pivot at the store center of gravity, thus reducing the store pitch moment on the wing due to inertial loads, maneuvers, and aerodynamic loads. The results of Fig. 9 show that the flutter velocity is increased while moving forward the pivoting point (increasing x_{fp}), tending asymptotically to an increase of 70% in the flutter velocity over the rigid-pylon flutter instability for $x_{fp} > 0.8$ and $\xi_p = 0$. The results of Fig. 9 show that increasing the damping coefficient lowers the flutter velocity of the system. The location of the pivot point for

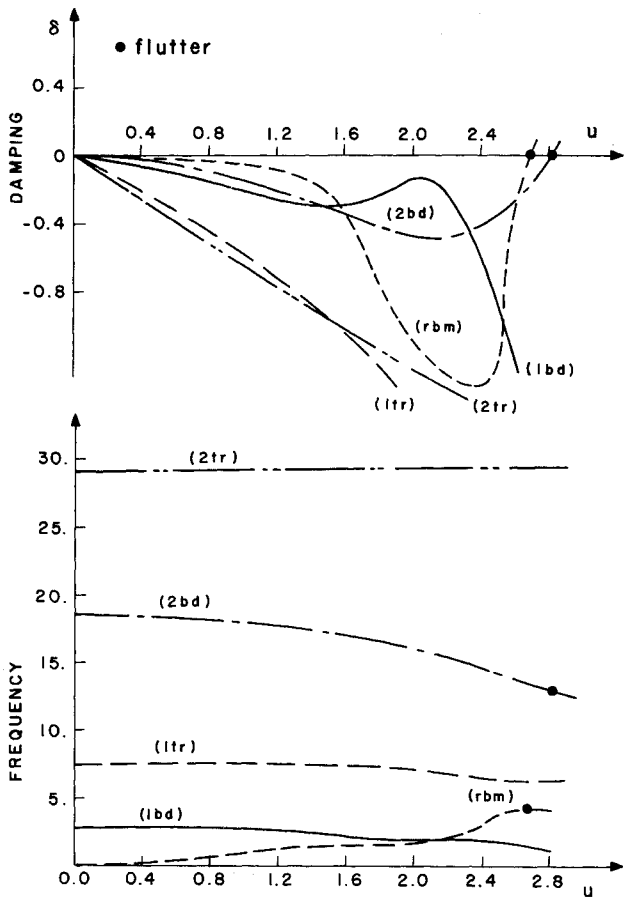

Fig. 10 Frequency and damping of the fundamental aeroelastic modes and rigid-body mode vs the dimensionless airspeed for a soft decoupler pylon mounted at the tip of an unswept wing ($\omega_p = 1$, $x_{fp} = 0.6$, $\xi_p = 0$).

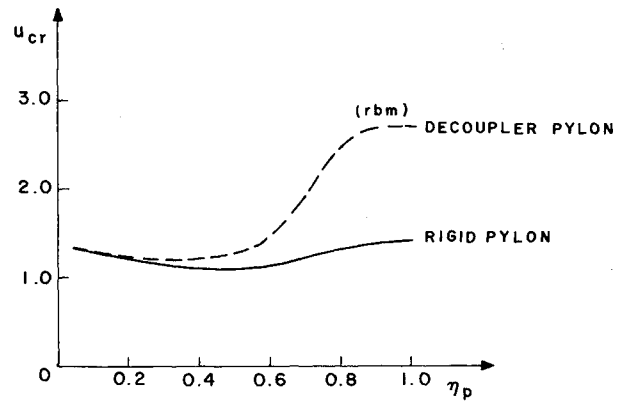

Fig. 11 Comparison study between the rigid pylon and a soft decoupler pylon of the variation of the critical velocity of the system vs the spanwise location of the decoupler pylon ($\omega_p = 1$, $\xi_p = 0$, $x_{fp} = 0.6$) for an unswept wing.

the pylon is frozen at the value $x_{fp} = 0.6$ for the rest of the parametric study reported hereafter.

Figure 10 illustrates the frequencies and damping of the modes vs flight velocity for a forward pivot point location for a soft decoupler pylon ($x_{fp} = 0.6$, $\omega_p = 1$, $\xi_p = 0$, and the pylon allocate at the tip $\eta_p = 1$). The results of Fig. 10 indicate that the rigid body mode (rbm) interacts with 1tr to undergo flutter instability. The second bending mode (2bd) mode also undergoes flutter instability at a slightly higher velocity than the flutter velocity of the rbm. It should be noted that the frequencies of 1bd and rbm cross (coalesce) without causing instability.[18]

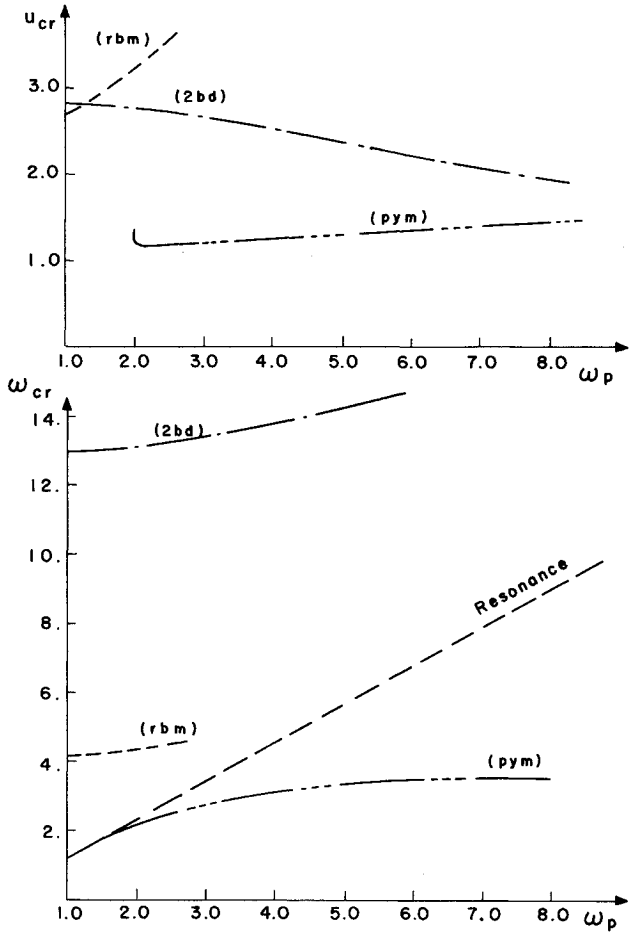

Fig. 12 Variation of the critical frequency and velocity of the system vs the natural frequency of the decoupler pylon's spring while the store is mounted at the tip of an unswept wing ($x_{fp}=0.6$, $\xi_p=0$).

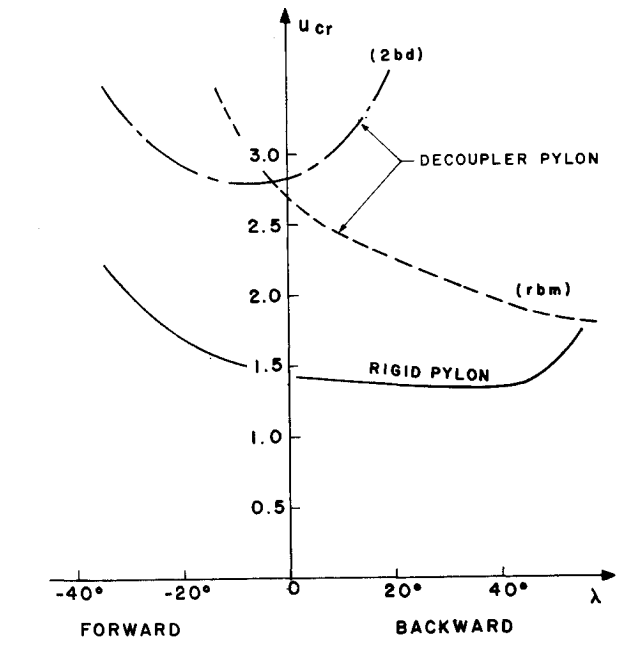

Fig. 13 Comparison study between the rigid pylon and a soft decoupler pylon of the variation of the critical velocity of the system vs the sweep angle of the wing ($\omega_p=1$, $x_{fp}=0.6$, $\eta_p=1$, $\xi_p=0$).

Figure 11 depicts the variation of the flutter velocity of the system vs the wing spanwise location of the pylon for a forward pivot point location ($x_{fp}=0.6$, $\omega_p=1$, and $\xi_p=0$). The

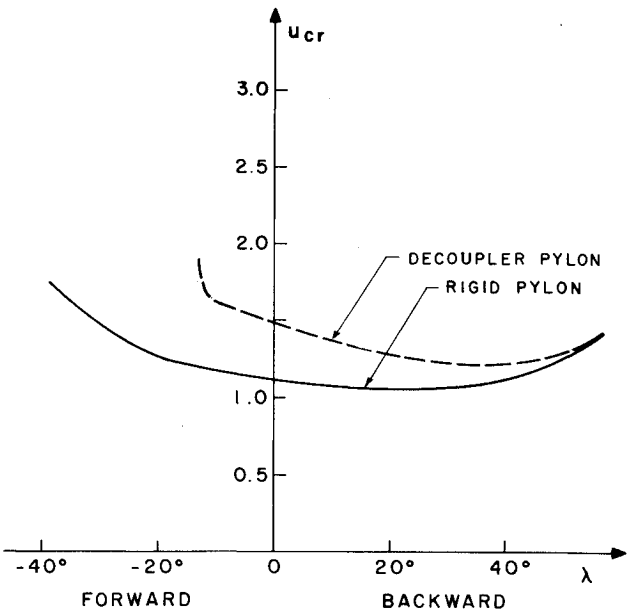

Fig. 14 Comparison study between the rigid pylon and a soft decoupler pylon of the variation of the critical velocity of the system vs the sweep angle of the wing ($\omega_p=1$, $x_{fp}=0.6$, $\eta_p=0.6$, $\xi_p=0$).

results shown in Fig. 11 indicate that the decoupler pylon is a very good passive flutter suppressor device for spanwise store station located toward the wing's tip. The effectiveness of the decoupler pylon diminishes as a flutter suppressor as the location of pylon is moved toward the wing's root ($\eta_p<0.5$). The flutter velocity of the 2bd mode is not plotted in Fig. 11 due to the fact that it fluttered at a higher velocity compared to the velocity of the rbm indicated in Fig. 11. The decoupler pylon behaves like a vibration absorber, which explains its ability to effectively suppress flutter when mounted at the wing's tip where the elastic vibration of the wing is more enhanced.

The critical velocity and frequency of the system for a forward pivot location ($x_{fp}=0.6$, $\xi_p=0$, and pylon allocate at the wing's tip $\eta_p=1$) vs the natural frequency of the decoupler pylon ω_p are shown in Fig. 12. The results of Fig. 12 indicate that, for the decoupler pylon to be an effective passive flutter suppressor, the natural frequency of the decoupler spring has to be less than two ($\omega_p<2$). The influence of angle of sweep of the wing and the cross-coupling stiffness on the flutter velocity characteristic of the system is analyzed hereafter.

Figure 13 depicts the influence of the angle of sweep of the wing on the flutter velocity instability of the system ($x_{fp}=0.6$, $\omega_p=1$, $\xi_p=0$) for a pylon mounted at the wing's tip ($\eta_p=1$). The flutter velocity of the system for a rigid pylon is indicated as reference. It is seen that the ability of the decoupler pylon to suppress the flutter velocity of the system declined as the sweep angle of the wing is increased backward. For a forward-swept wing (FSW) ($\lambda<-3$ deg), the flutter of the 2bd mode determines the velocity instability of the system. The ability of the decoupler pylon to suppress flutter is impressive for the FSW configuration.

Figure 14 demonstrates the variation of the flutter velocity of the system ($\omega_p=1$, $x_{fp}=0.6$, and $\xi_p=0$) vs the sweep angle of the wing for a pylon located at 60% span ($\eta_p=0.6$). It is seen that the decoupler pylon is able to eliminate flutter for a FSW ($\lambda<-14$ deg), but is doing a very poor job for a backward-swept wing.

Aeroelastic tailoring relies upon interaction or coupling between shear strain and normal strains such as might be found in anisotropic laminate (or an orthotropic laminate rotated with respect to some reference axis; see Fig. 2b). Such normal/shear strain coupling leads to coupling between

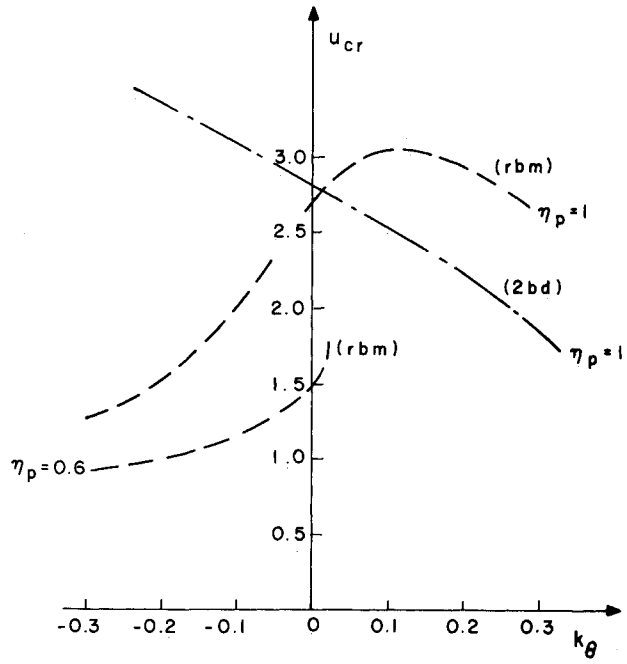

Fig. 15 Variation of the critical velocity of the system vs the cross-coupling stiffness coefficient for a soft decoupler pylon located at two different spanwise wing's stations ($\eta_p=0.6$ and 1) for an unswept wing ($\omega_p=1$, $x_{fp}=0.6$, $\xi_p=0$).

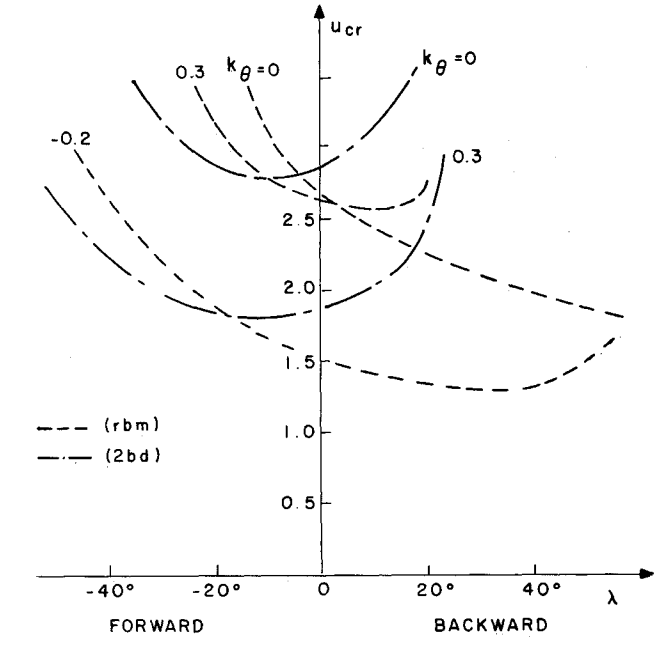

Fig. 16 Variation of the critical velocity of the system vs the sweep angle of the wing for various values of the cross-coupling stiffness coefficient for a soft decoupler pylon mounted at the wing's tip ($\omega_p=1$, $x_{fp}=0.6$, $\xi_p=0$).

bending deformation and twisting rotation about a reference axis when loads are applied along this axis. The coupling between bending and torsion is introduced in the analysis through the D_{26} flexural moduli [see Eq. (2)], which upon integration became the K parameter (k_θ dimensionless). Figure 15 illustrates the influence of the bending torsion cross-coupling stiffness on the flutter velocity of the unswept wing ($x_{fp}=0.6$, $\omega_p=1$, $\xi_p=0$, and $\lambda=0$) for two wing spanwise locations of the pylon ($\eta_p=1$ and 0.6). It is seen that slightly positive cross-coupling stiffness ($k_\theta>0.025$) can eliminate flutter for the $\eta_p=0.6$ case. The results for the $\eta_p=1$ case indicate that positive cross-coupling stiffness considerably lowers the flutter velocity of the 2bd mode, while negative cross-coupling stiffness appreciably lowers the flutter velocity of the rbm mode. The results of Fig. 15 indicate that, for the unswept wing, a slightly positive cross-coupling stiffness ($k_\theta\sim0.03$) may be beneficial for the decoupler pylon located at $\eta_p=0.6$ as well as for the $\eta_p=1$ case.

Figure 16 depicts the combined effect of the cross-coupling stiffness and the sweep angle of the wing on the flutter velocity of the system for a pylon mounted at the wing's tip. The results of Fig. 16 show the complexity of the aeroelastic stability behavior of the system, while investigating the influence of two parameters of major importance: sweep angle of the wing and cross-coupling stiffness.

It should be noted that, due to the many parameters causing the coupling between the bending, torsion, and rigid-body modes, it is very difficult to draw general conclusions. Furthermore, the example tested has a single lifting surface, while an aircraft usually has more than one lifting surface. The horizontal tail or canard aerodynamics may significantly affect the rigid-body modes and thus the coupling with the elastic modes of the wing. The method may be applied to a more realistic configuration without extensive modifications and effort.

Conclusions

A simple and effective analytical model to investigate the concept of the ability of the decoupler pylon to suppress wing/store flutter is introduced. A rectangular wing with a single store is used as a basis for the study, while including the rigid-body modes of the aircraft in the analysis. Despite the limitations imposed upon the study by the model's restriction assumptions, it seems that the model contains essential features that enable the study of the stability behavior of the system. The rigid-body modes of the aircraft plays an essential roll in the stability behavior of the wing/store configuration. The study indicates that the decoupler pylon is an effective passive flutter suppressor device and that its ability to suppress flutter is affected by many parameters besides the stiffness of the decoupler pylon spring. The location of the pylon's pivot point, the spanwise location of the decoupler pylon, and the angle of sweep of the wing are some of the parameters that considerably affect the dynamic behavior of the system. Furthermore, it is shown that the aeroelastic tailoring of the wing has a major influence on the flutter instability of the configuration.

References

[1]Mykytow, W.J., "Recent Analysis Methods for Wing Store Flutter," *Specialist Meeting on Wing-With-Stores Flutter,* AGARD CP-162, April 1962.

[2]Foughner, J.T. Jr. and Besinger, C.T., "F-16 Flutter Model Studies External Wing Stores," NASA TM-74078, Oct. 1977.

[3]Katz, H., "Flutter of Aircraft with External Stores," *Proceedings of Aircraft Stores Symposium,* Vol. II, Armament Development and Test Center, Elgin Air Force Base, FL, Nov. 1969.

[4]Reed, W.H., Foughner, J.T., and Runyan, H.L., "Decoupler Pylon: A Simple, Effective Wing/Store Flutter Suppressor," *Journal of Aircraft,* Vol. 17, March 1980, pp. 206–211.

[5]Nissim, E., "Flutter Suppression Using Active Controls Based on the Concept of Aerodynamic Energy," NASA TN D-6199, 1971.

[6]Sandford, M.C., Abel, I., and Gray, D.L., "Development and Demonstration of a Flutter Suppression System Using Active Controls," NASA TR R-450, Dec. 1975.

[7]Hollinger, H., "Active Flutter Suppression on an Airplane with Wing-Mounted External Stores," *Structural Aspect of Active Controls,* AGARD CP-228, Aug. 1977.

[8]Noll, T.E., Huttsell, L.J., and Cooley, D.E., "Wing/Store Flutter Suppressor Investigation," *Journal of Aircraft,* Vol. 18, Nov. 1981, pp. 969–975.

[9]Cazier, F.W. and Kehoe, M.W., "Flight Test of Passive Wing/Store Flutter Suppressor," *1986 Aircraft/Stores Compatibility*

Symposium, Wright-Patterson Air Force Base, OH, April 1986.
[10]Ashton, J.E. and Whitney, J.M., *Theory of Laminated Plates,* Technonic, Stamford, CT, 1970.
[11]Lottati, I., "Aeroelastic Stability Characteristics of Composite Swept Wing with Tip Weights for an Unrestrained Vehicle," *Journal of Aircraft,* Vol. 24, Nov. 1987, pp. 793-802.
[12]Turner, C.D., "Effect of Store Aerodynamics on Wing/Store Flutter," *Journal of Aircraft,* Vol. 19, July 1982, pp. 574-580.
[13]Green, J.A., "Aeroelastic Tailoring of Composite Wings with External Stores," AIAA Paper 86-1021, 1986.
[14]Bisplinghoff, R.L., Ashley, H., and Halfman, R.L., *Aeroelasticity,* Addison-Wesley, Reading, MA, 1955, Chap. 7.
[15]Lottati, I., "Flutter and Divergence Aeroelastic Characteristics for Composite Forward Cantilevered Wing," *Journal of Aircraft,* Vol. 22, Nov. 1985, pp. 1001-1007.
[16]Goland, M. and Luke, Y.L., "The Flutter of a Uniform Wing with Tip Weights," *Journal of Applied Mechanics,* Vol. 15, No. 1, March 1948, pp. 13-20.
[17]Housner, J.M. and Stein, M., "Flutter Analysis of Swept-Wing Subsonic Aircraft with Parameter Studies of Composite Wings," NASA TN D-7539, Sept. 1975.
[18]Nissim, E. and Lottati, I., "On Optimization Method for the Determination of the Important Flutter Modes," *Journal of Aircraft,* Vol. 18, Aug. 1981, pp. 663-668.